Study of the Ni–$NiAl_2O_4$–YSZ cermet for its possible application as an anode in solid oxide fuel cells

2006 J. Phys.: Condens. Matter 18 4685

(http://iopscience.iop.org/0953-8984/18/19/020)

INSTITUTE OF PHYSICS PUBLISHING JOURNAL OF PHYSICS: CONDENSED MATTER

J. Phys.: Condens. Matter **18** (2006) 4685–4696 doi:10.1088/0953-8984/18/19/020

Study of the Ni–$NiAl_2O_4$–YSZ cermet for its possible application as an anode in solid oxide fuel cells

A Reyes-Rojas[1,2], H E Esparza-Ponce[1] and J Reyes-Gasga[3]

[1] Centro de Investigación en Materiales Avanzados SC, Miguel de Cervantes 120, Complejo Industrial Chihuahua, Chihuahua, Mexico
[2] Universidad Autónoma del Estado de México, Facultad de Química, Toluca, Mexico
[3] Universidad Nacional Autónoma de México, Instituto de Física, México DF, Mexico

E-mail: armando_reyesmx@yahoo.com.mx

Received 26 October 2005, in final form 4 April 2006
Published 27 April 2006
Online at stacks.iop.org/JPhysCM/18/4685

Abstract

Nanocrystalline Ni–$NiAl_2O_4$–YSZ cermet with a possible application as anode in solid oxide fuel cells (SOFCs) has been developed. The powders were prepared by using an alternative solid-state method that includes the use of nickel acetylacetonate as an inorganic precursor to obtain a highly porous material after sintering at 1400 °C and oxide reduction (NiO–Al_2O_3–YSZ → Ni–$NiAl_2O_4$–YSZ) at 800 °C for 8 h in a tubular reactor furnace using 10% H_2/N_2. Eight samples with 45% Ni and 55% Al_2O_3–YSZ in concentrations of Al_2O_3 oxides from 10 to 80 wt% of were mixed to obtain the cermets. The obtained material was compressed using unidirectional axial pressing and calcinations from room temperature to 800 °C. Good results were registered using a heating rate of 1 °C min^{-1} and a special ramp to avoid anode cracking. Thermal expansion, electrical conductivity, and structural characterization by thermo-mechanical analyser (TMA) techniques/methods, the four-point probe method for conductivity, scanning electron microscopy (SEM), x-ray energy dispersive spectroscopy (EDS), x-ray diffraction (XRD), and the Rietveld method were carried out. Cermets in the range 5.5 to 11% Al_2O_3 present a crystal size around 200 nm. An inversion degree (I) in the $NiAl_2O_4$ spinel structure of the cermets Ni–$NiAl_2O_4$–YSZ was found after the sintering and reduction processes. Good electrical conductivity and thermal expansion coefficient were obtained for the cermet with 12 wt% of spinel structure formation.

1. Introduction

Fuel-cell systems for heat and electricity generation will be introduced in the near future in order to reduce energy cost. A solid oxide fuel cell (SOFC) would eliminate the need of an

external gas reformer compared with polymer electrolyte fuel cells (PEM) when applied to residential and industrial applications [1]. The anode material commonly used in SOFCs is Ni–YSZ, which is operated between 600 and 1000 °C [2–4].

It is known that the efficiency of the anode materials depends mainly on the physical union of triple phase boundaries and a porosity of around 40% [5–7]. Ni is used because of its excellent electro-catalytic activity for H_2 oxidation reaction, high electrical conductivity, and high stability with YSZ electrolyte [8, 9]. However, in SOFC system applications many other materials have also been studied in order to reduce operating temperature, manufacturing processes, and anode cost [10–12]. As an alternative, Ni–YSZ can be used with additions of Al_2O_3, which can give rise to the $NiAl_2O_4$ spinel structure [13].

Studies of Ni/Al_2O_3 materials with addition of noble metals such as Pt, Pd, and Ir were evaluated for reforming crude ethanol and methane for H_2 production [14, 15]. Other studies were carried out to study the catalytic properties of $Ni/Al_2O_3 \rightarrow NiAl_2O_4$ during the reactions related to methane oxidative steam reforming and combustion for hydrogen production [16, 17]. The key issue here is to evaluate the characteristics of thermal expansion and electrical conductivity in anodes Ni–YSZ–$NiAl_2O_4$.

It is known that the $NiAl_2O_4$ structure can present an inversion degree [18, 19]. The inversion degree (I) is related to the following relation:

$$(A_{1-x}B_x)[A_xB_{2-x}]O_4 \tag{1}$$

x is the inversion degree (I); A is the Ni^{2+} ions; B is the Al^{3+} ions.

The difference of the Ni–$NiAl_2O_4$–YSZ ratio can affect the anode properties, such as the thermal expansion coefficient behaviour of the sintered materials and the reductions in H_2 atmosphere. More recent works on the $NiAl_2O_4$ spinel structure at high temperature [20] and high pressure [21] suggest that the (I) can be changed from 0.8 to 0.99. This shows that, from high temperature, the $NiAl_2O_4$ spinel structure is preserved after the material is cooled down.

In this work, the electrical conductivity, the thermal expansion coefficients, and the structural analysis of Ni–YSZ performance, co-doped with the Al_2O_3 system, are presented. Microstructure correlation, porosity and electrical conductivity at constant temperature will be discussed. The inversion degree of $NiAl_2O_4$ and its relation with the characteristic properties of Ni–$NiAl_2O_4$–YSZ for its possible application as an anode in the SOFC system will also be commented on.

2. Experimental procedure

Eight Ni–$NiAl_2O_4$–YSZ cermets were prepared using high-purity precursors, nickel acetylacetonate (NiAA), YSZ (8 mol% yttrium) with >99.9% purity (Aldrich), and Al_2O_3 with >99.5% (Baikalox). NiAA and NiO were added in adequate concentrations to obtain 45% Ni, and 55% of Al_2O_3–YSZ in the concentrations ranging from 10 to 80 wt% of Al_2O_3. NiAA organic content was used as the pore-former in all cermets, which maintains the pore volume constant throughout the sample. The compositions for the eight samples are shown in table 1.

Powders of each pure sample (series A) were hand-ground in an agate mortar for 1 h, and the obtained powders were compressed into 1 cm diameter and 1 mm thick discs using a 1 ton unidirectional axial pressure for 5 s, and drying them at 110 °C for 12 h. Afterwards, the discs were calcined with a heating rate of 3 °C min^{-1} in an atmospheric air-heated box furnace from room temperature to the ramps 200 °C (1 h), 350 °C (1 h), and 400 °C (1 h) to 800 °C for 2 h. Once the pores were formed, the discs were sintered at 1400 °C for 2 h with a heating rate of 5 °C min^{-1}. The cooling rate was 5 °C min^{-1} in all of them. Once the sintered samples were obtained, each one was reduced in a horizontal furnace at 800 °C under 10% H_2 in N_2

Table 1. Composition of the eight samples for the Ni–$NiAl_2O_4$–YSZ composites.

Sample	45 wt% Ni	55 wt%		α (μm m^{-1} °C^{-1})
		Al_2O_3	YSZ	24–800 °C
A1	45	5.5	49.5	14.5
A2	45	11	44	13
A3	45	16.5	38.5	12
A4	45	22	33	11.5
A5	45	27.5	27.5	10.5
A6	45	33	22	10
A7	45	38.5	16.5	9.5
A8	45	44	11	9.0

atmosphere with a flow ≈300 cm^3 min^{-1}. We kept the reducing atmosphere during cooling to inhibit the formation of oxidation layers on the cermet surface.

After the reduction process, each sample was placed in the x-ray powder diffractometer, model X'Pert MPD (Phillips), equipped with Cu Kα monochromatic radiation, and θ–2θ geometry, using a 2θ angle range from 20° to 80° in step-scanning mode with a step length of 0.05° and using a step-counting time of 10 s. Structure parameters were obtained by the Rietveld method with the FULLPROF program [22], and a peak shape modified Thompson–Cox–Hasting pseudo-Voigt function for the calculated reflection profile. Reproducibility for the (a) background parameters, (b) scale factors, (c) instrumental effects (zero point and sample off centring), (d) structural parameters, (e) profile parameters, (f) domain size parameters, and (g) phase quantification was considered for refinement until the results converged into minimum values. Instrumental broadenings U, V, and W were determined from the Rietveld refinement of an x-ray diffraction pattern of the Al_2O_3 powder sample (a standard for quantitative analysis in XRD) [23]. The results were used in the refinement of all the patterns. The calculated values were $U = 0.013\,01$, $V = -0.030\,281$, and $W = 0.010\,934$. The determination of the domain size (or crystal size) was done considering the broadening of the Bragg reflection profile. All data for the crystallographic analysis were obtained from well known references [24–26].

Crystallographic density (ρ_c) was calculated from the volume data obtained by the Rietveld analysis, and then used to calculate the porosity (p) of the sample using the equation

$$p = 1 - \rho * \rho_c^{-1} \tag{2}$$

where ρ is the bulk density.

The micro-structural evolution and chemical composition data of the cermets were obtained using a JEOL-5600 scanning electron microscope (SEM) in which EDS EDAX equipment is attached. To do this, the sample discs were stuck onto a conductive copper tape and sputtered with a thin layer of a Au–Pd alloy to prevent electron charging. Thermal expansion coefficients were determined with a thermo-mechanical analyser (TMA) model 2920 (TA Instruments). All the samples were exposed to a temperature gradient of 10 °C min^{-1}, under 10% H_2 in N_2 atmosphere, with a flow ≈300 cm^3 min^{-1}. A special sample of the YSZ–Ni (45 wt% Ni) cermet was prepared to be compared with the Ni–$NiAl_2O_4$–YSZ cermets.

Using conventional techniques of metallographic preparation, the discs were polished on both flat sides and using colloidal alumina in the last step to obtain good surface quality. Electrical conductivity of Ni–$NiAl_2O_4$–YSZ cermets was measured with the four-point probe Van Der Pauw method at 800 °C. Four gold wire (Alfa Aesar, 99.999%) electrodes were pressed together with platinum sheets between two ceramic plates using four screws to avoid electrical contact between electrodes. The measurements were performed in a continuous 10% H_2 in N_2

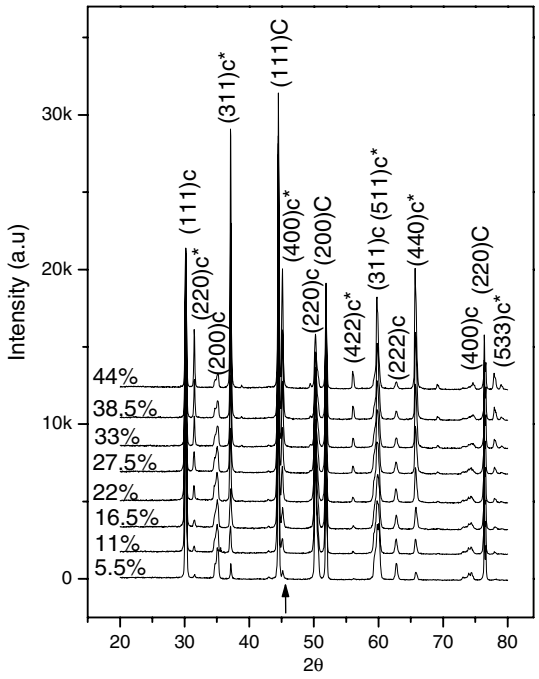

Figure 1. X-ray diffraction patterns of the Ni–$NiAl_2O_4$–YSZ composites after the reduction process. The arrow shows the beginning of formation of the cubic $NiAl_2O_4$ spinel structure (C Ni structure, c* $NiAl_2O_4$, c YSZ).

atmosphere (Praxair, 99.9%), with a flow ≈300 cm^3 min^{-1}, inside a horizontal tubular furnace and using Agilent 34401 A digital multimeters.

3. Results and discussion

3.1. Rietveld analysis

The XRD patterns of Ni–$NiAl_2O_4$–YSZ cermets after sintering at 1400 °C for 2 h and reduction to 800 °C with H_2–N_2 atmosphere for 8 h (figure 1) clearly confirm the formation of the $NiAl_2O_4$ spinel structure and the absence of NiO crystals. Figure 1 also shows the effect of Al_2O_3 variation in the cermets and the arrow indicates the peak (400) of the $NiAl_2O_4$ spinel structure. When the amount of alumina increases, the spinel structure increases too, and the Ni crystallographic reflection decreases. This is attributed to an increase in the formation of solid solution $NiAl_2O_4$. However, some differences are found in the $NiAl_2O_4$ relative intensity, indicating an inversion degree (I) [27].

The Rietveld refinement for the cermets (series A) was obtained using the space group $Fm\bar{3}m$ for the YSZ cubic phase, $Fd\bar{3}m$ for the $NiAl_2O_4$ cubic phase, and $Fm\bar{3}m$ for the NiO and Ni cubic unit cells [28]. Figure 2 shows the case for sample A7 (27% Ni) after the reduction process as example of the final pattern fitting, and it indicates an almost flat difference between the observed and calculated profile intensities. The experimental profile was indicated by (+), the calculated by (−), and the difference plot between the observed and calculated intensities is shown in each case. All the samples showed similar behaviour. The adjustment degree for fitting patterns was from 5 to 10 (R_{wp}) [20].

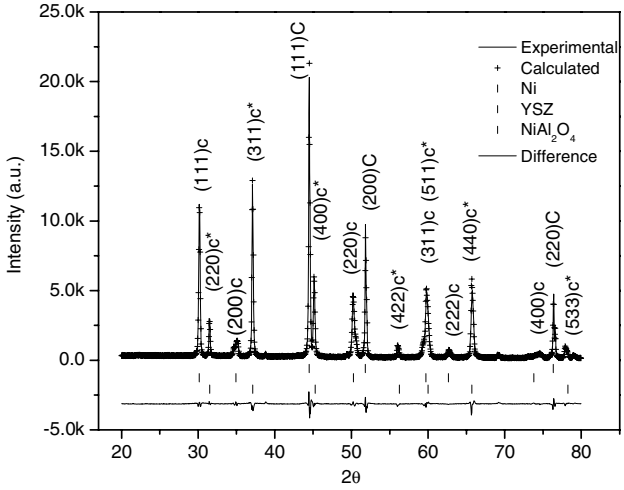

Figure 2. Example of the experimental and the calculated XRD pattern by Rietveld refinement for sample A7 after reduction. The experimental profile is indicated by (+), the calculated by (−). The difference plot between the observed and calculated intensities is also shown.

Table 2 summarizes the crystallographic data obtained after the Rietveld refinement and the relative phase abundance in each cermet. Note that the $NiAl_2O_4$ phase content increases from 6 to 67 wt% when Ni decreases to almost half of the initial value (22 wt%), although some differences were observed for the average domain size of Ni crystals. These percentages represent the variation of Al_2O_3 in YSZ from 10 to 80%.

Domain size for the samples A1, A2 and A3 increased from 100 to 400 nm but for the rest of the samples it increased to >1000 nm. However, the domain size for the $NiAl_2O_4$ and YSZ structure did not change considerably during the reduction process; neither did the lattice parameter and volume size for the Ni and YSZ structures. This change is similar to the one reported by other authors [29–31]. Different results were obtained in the lattice parameters for the $NiAl_2O_4$ spinel structure, which indicated a volume size decrease. This is consistent with the change in the relative position and intensity of reflections *hkl* for spinel structure: the volume decreases when the $NiAl_2O_4$ content increases.

3.2. Inversion degree

Figure 3 shows the comparison between the unit cell parameter *a* and the positional parameter O (oxygen) versus wt% $NiAl_2O_4$ contents. Note in this figure that *a* decreases when the $NiAl_2O_4$ content increases. This result can be explained by the crystallographic expansion produced during the larger Ni^{2+} ion displacement (8a) in the tetrahedral site to the (16d) octahedral site while Al^{3+} ions (16d) move to (8a) sites. Other authors have reported a similar behaviour [32]. The atomic position of O varies from 0.278 to 0.262, which is also consistent with the decrease of the *a* cell edge. The Rietveld analysis suggests that $NiAl_2O_4$ contents are inversely proportional to the cell volume and directly proportional to the inversion degree (figure 4) in cermets Ni–$NiAl_2O_4$–YSZ after sintering at 1400 °C for 2 h and reduction to 800 °C with H_2–N_2 atmosphere for 8 h. Figure 4 also shows that the inversion degree (I) varies from 0.81 to 0.95. These results indicate that $NiAl_2O_4$ normal spinel structure ($x = 0$) can vary from $(Ni_{0.19}Al_{0.81})[Ni_{0.81}Al_{1.19}]O_4 \Leftrightarrow NiAl_2O_4$ to $(Ni_{0.05}Al_{0.95})[Ni_{0.95}Al_{1.05}]O_4 \Leftrightarrow NiAl_2O_4$ in the solid solution of Ni–$NiAl_2O_4$–YSZ cermets. Similar behaviour has been reported in

Table 2. Crystal structure data of the Ni–$NiAl_2O_4$–YSZ cermets obtained after the Rietveld refinement. The relative phase abundance in each cermet is also shown. (Note: The number between parentheses represents the error of the last number.)

		Sample							
		A1	A2	A3	A4	A5	A6	A7	A8
Phase (wt%)	Ni	49(2)	47(1)	37(1)	34(1)	32(2)	30(1)	27(1)	22(1)
	$NiAl_2O_4$	6(2)	12(1)	25(1)	36(1)	43(2)	50(1)	58(1)	67(1)
	YSZ	45(1)	41(1)	38(1)	30(1)	25(1)	20(1)	15(1)	11(1)
Domain size (nm)	Ni	100(1)	180(2)	420(5)	810(2)	>1000	>1000	>1000	>1000
	$NiAl_2O_4$	50(5)	60(4)	100(3)	100(5)	125(2)	130(4)	180(2)	200(2)
	YSZ	150(4)	150(2)	145(3)	160(4)	200(4)	210(4)	212(2)	250(5)
Lattice (Å)	Ni	3.5236(1)	3.5233(2)	3.5233(1)	3.5235(2)	3.5232(1)	3.5236(1)	3.5235(1)	3.5234(1)
	$NiAl_2O_4$	8.0261(1)	8.0248(2)	8.0219(1)	8.0201(2)	8.0199(1)	8.0191(1)	8.0182(3)	8.0179(1)
	YSZ	5.1292(2)	5.1291(1)	5.1392(1)	5.1293(1)	5.1291(2)	5.1291(1)	5.1292(2)	5.1392(2)
Volume ($Å^3$)	Ni	43.739(1)	43.739(1)	43.739(1)	43.744(1)	43.733(1)	43.749(1)	43.744(1)	43.741(1)
	$NiAl_2O_4$	517.027(1)	516.776(2)	516.216(1)	515.868(2)	515.831(1)	515.675(1)	515.502(3)	515.444(1)
	YSZ	134.944(1)	134.934(2)	134.944(1)	134.951(1)	134.934(2)	134.934(2)	134.944(1)	134.944(1)
Porosity		47(2)	45(2)	44(2)	43(1)	42(1)	42(1)	41(1)	41(2)

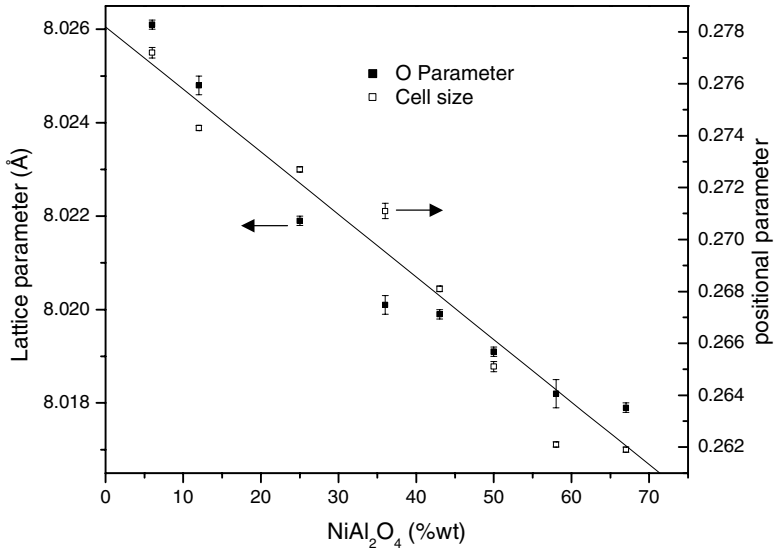

Figure 3. Graph of the lattice parameter a and the positional oxygen parameter behaviours as a function of the content of $NiAl_2O_4$. Note that a decreases when the content of $NiAl_2O_4$ increases.

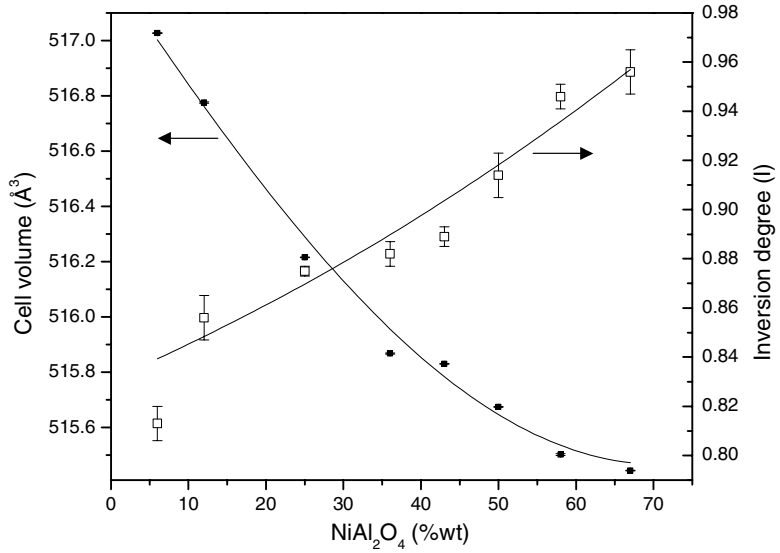

Figure 4. Graph of the cell volume a^3 and I inversion degree behaviours as a function of $NiAl_2O_4$ content. The arrows indicate the corresponding reading axes for each case.

other works [20, 21]. The values are almost $I \approx 1$ or total inversion when $NiAl_2O_4$ content is closed to 67%.

Figure 5 shows a plot of the effect of SOF (site occupancy factor) for Ni (left) and Al (right) in spinel structure versus inversion degree and cell volume. Ni and Al occupancy shows a symmetrical and simultaneous increment in inversion degree due to the interchange and movement of cations only. Subsequently, a behaviour of slow rate increase for the cell

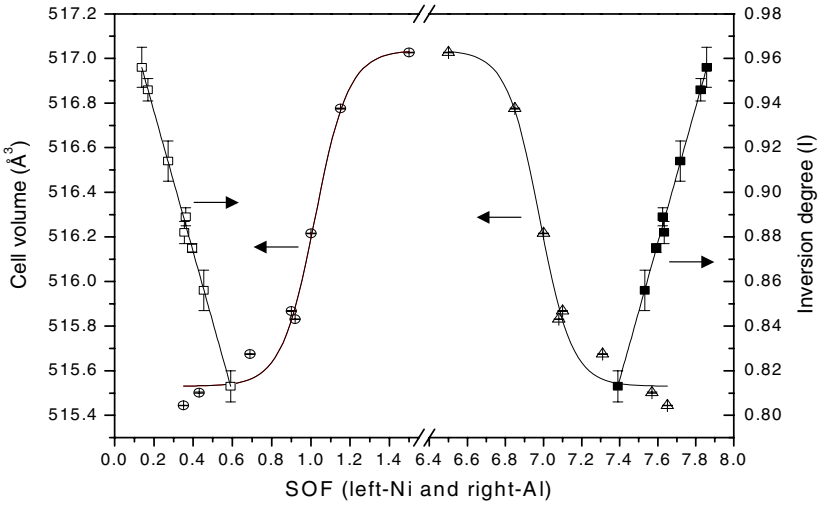

Figure 5. Variation of SOF (left—Ni and right—Al) versus cell volume and inversion degree in spinel structure. Occupancy of Ni cation (□, ○); occupancy of Al cation (■, △). The arrows indicate the corresponding reading axes for each case.

volume was observed. When SOF is 0.35 and 7.65 for Ni and Al respectively, the cell volume is 515.444 Å^3 (67 wt% of $NiAl_2O_4$ in the cermets) for an SOF of 1.5 and 6.5 for Ni and Al respectively, and increases to 517.027 Å^3 (6 wt% of $NiAl_2O_4$). This behaviour can be explained through the cation interchange, which is ordered in a more close-packed spinel structure when the $NiAl_2O_4$ content increases in the Ni–$NiAl_2O_4$–YSZ cermets.

3.3. Microstructure and porosity

The microstructures of all the cermets observed with SEM before and after the reduction process were very similar. Figures 6 and 7 show the microstructure for the Ni–$NiAl_2O_4$–YSZ composites 5.5, 11, 16.5 and 22 wt% Al_2O_3, and 27.5, 33, 38.5 and 44 wt% Al_2O_3 respectively after the reduction process. As can be seen in these SEM images, the particles of these samples show a very homogeneous form, and they are nearly spherical. The Ni, $NiAl_2O_4$ distribution and YSZ particles are very homogeneous. Similar microstructure was reported in anodes for SOFC applications by other authors [33, 34]. Crystal agglomerates are approximately 1 μm in size, smaller than for the first samples (figure 6). However, for the second series of the Ni crystals, these agglomerates increase to around 7 μm. This was confirmed by characteristic x-ray EDS analysis, which showed that the large crystal agglomerates observed consisted of single Ni phase.

Anode porosity was found to be inversely proportional to the amount of $NiAl_2O_4$ and directly proportional to NiO phase in the sample. For example, the porosity for sample with 6% of $NiAl_2O_4$ was almost 47% [35] and for 67% it was 41%. The increment of porosity is associated with NiAA and NiO decomposition during the calcinations and reduction process. This can be explained easily by the change in volume size registered during the reduction process because it is a function of the amount of NiO available to give and increment the porosity. As seen in the SEM images (figures 6 and 7), there is an inverse relationship between the pore size and the $NiAl_2O_4$ content: when the $NiAl_2O_4$ content increases, the pore size

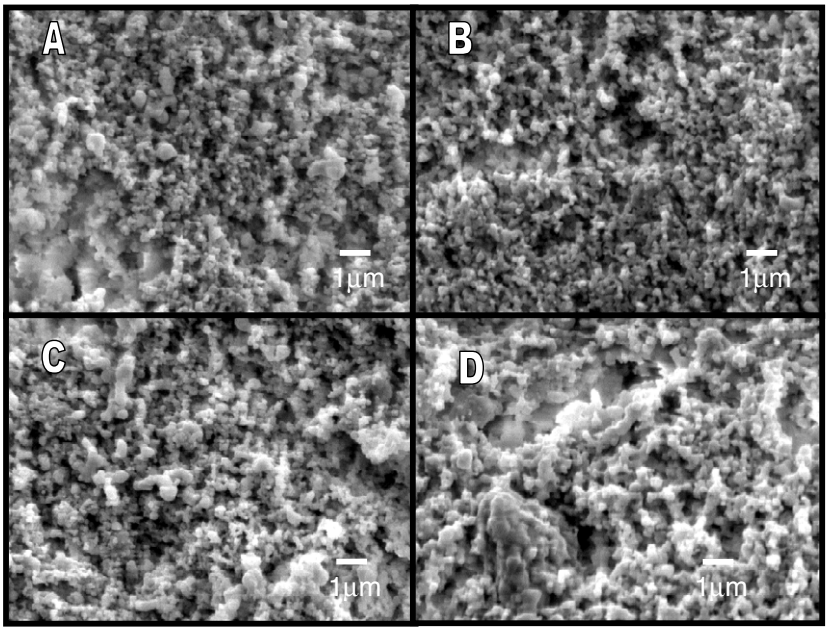

Figure 6. SEM images of Ni–$NiAl_2O_4$–YSZ composites with the concentration of Al_2O_3 of 5.5 (a), 11 (b), 16.5 (c) and 22 wt% (d) after reduction.

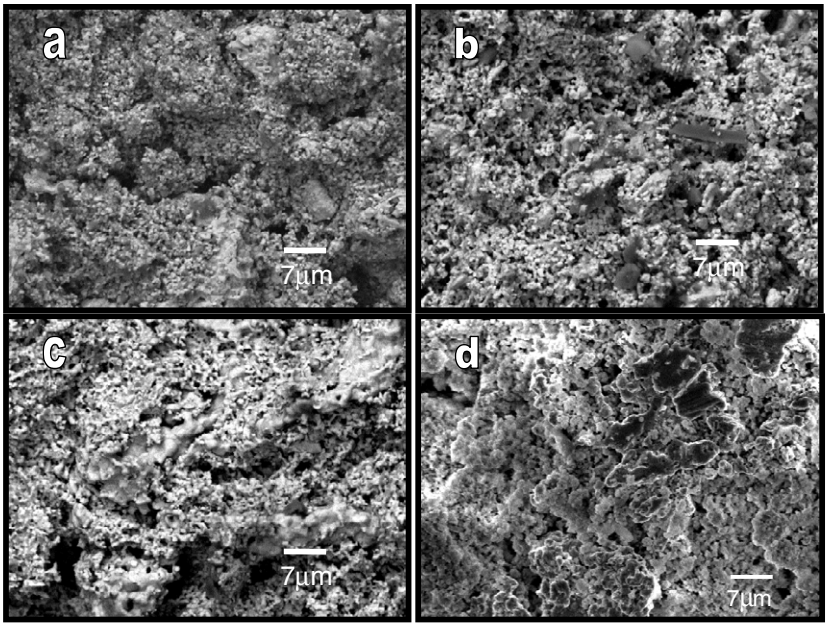

Figure 7. SEM images of Ni–$NiAl_2O_4$–YSZ composites with the concentration of Al_2O_3 of 27.5 (a), 33 (b), 38.5 (c), and 44 wt% (d) after reduction.

of the cermets goes smaller. This point is consistent with the results obtained with Rietveld refinement.

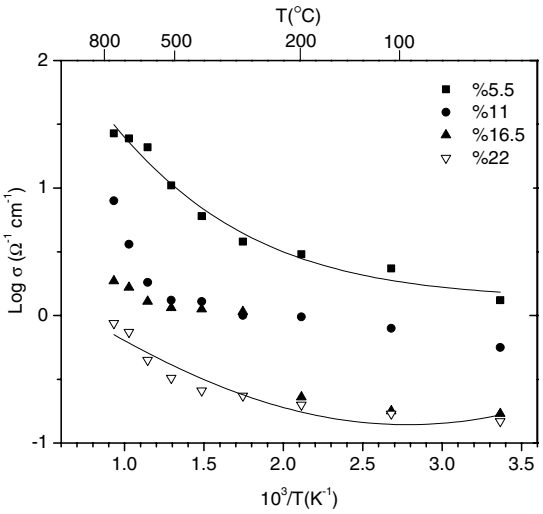

Figure 8. Log versus $1/T$ graphs for Ni–$NiAl_2O_4$–YSZ cermets at 800 °C with H_2–N_2 atmosphere.

3.4. The thermal expansion coefficient and electrical conductivity

The thermal expansion coefficient (α) behaviour in pure Ni–$NiAl_2O_4$–YSZ cermets sintered at 1400 °C for 2 h is shown in table 1. The thermal expansion of the cermets was between 0.75% and nearly 1.1% in the temperature range 25–800 °C with H_2–N_2 atmosphere. The maximum thermal expansion ($\approx$14.5 μm m^{-1} °C^{-1}) was registered in the cermet with 6 wt% of $NiAl_2O_4$. Cermets showed a positive thermal expansion up to 800 °C and α was inversely proportional to the $NiAl_2O_4$ spinel content. When the $NiAl_2O_4$ content was 67 wt%, the thermal expansion coefficient was $\alpha = 9$ μm m^{-1} °C^{-1}. These results allow us to conclude that the maximum change of α must be attributed to the abundance of Ni and YSZ. The thermal expansion coefficient for the special Ni–YSZ sample was $\alpha = 13$ μm m^{-1} °C^{-1}, which is consistent with the values reported by other authors [36]. The Ni–$NiAl_2O_4$–YSZ cermet with 47 wt% Ni was the one similar and consistent with this value.

Electrical conductivity at 800 °C was measured as a function of the Al_2O_3 content with respect to the YSZ content for all sintering composites, and a direct effect of the $NiAl_2O_4$ phase formation on the electrical properties of the cermets was found. The electrical conductivity behaviour of some of the cermets is plotted in figure 8. This figure only represents the electrical behaviour for the samples from 5.5 to 22 wt% of Al_2O_3. The samples from 27.5 to 44 wt% of Al_2O_3 increase their resistance considerably from 2 to 300 Ω approximately. The change of electrical conductivity in figure 8 can be attributed to the decrement of Ni and YSZ structure content, because when the nickel and YSZ decreases the electrical conductivity does too [37, 38]. When the phase formation of the $NiAl_2O_4$ does not go over 25% the electrical conductivity is similar to the anodes of Ni–YSZ in the range from 10% to 45 wt% of Ni, and this can vary from -1 to 2 [log(Ω^{-1} cm^{-1})] as indicated in [39, 40].

4. Conclusion

Composites of Ni–$NiAl_2O_4$–YSZ cermets with good electrical and thermal expansion properties and with possible application as anode in solid oxide fuel cells were synthesized.

The size lattice parameters of Ni and YSZ did not change during the whole process; however, the spinel structure volume decreased, because the inversion degree (I) changed. The atomic position of oxygen varies from 0.278 to 0.262, which is consistent with the change of the inversion degree and volume of the cell. The inversion degree varies from 0.81 to 0.95 in cermets Ni–$NiAl_2O_4$–YSZ after the sintering and reduction process. The results of electrical conductivity and thermal expansion coefficient in Ni–$NiAl_2O_4$–YSZ anodes, compared with the special sample (Ni–YSZ), and in agreement with other works, allow us to conclude that the samples with 6 and 12 wt% of $NiAl_2O_4$ phase are the most acceptable material for application as anode in the solid oxide fuel cell due to their similar performance.

Acknowledgments

We thank D Lardizabal, for their technical support, and to Facultad de Química, Universidad Autónoma del Estado de México, and the Centro de Investigación en Materiales Avanzados S.C. for the equipment and facilities.

References

[1] Hibino T, Hashimoto A, Yano M, Suzuki M, Yoshida S-I and Sanob M 2002 *J. Electrochem. Soc.* **149** A133–6
[2] Liu Y L, Sprimdahl S and Mogensen M 2003 *Solid State Ion.* **161** 1–10
[3] Fukui T, Ohara S, Naito M and Nogi K 2002 *J. Power Sources* **110** 91–5
[4] Koh J-H, Yoo Y-S, Park J-W and Lim H C 2002 *Solid State Ion.* **149** 157–66
[5] O'Hayre R, Barnett D M and Prinz F B 2005 *J. Electrochem. Soc.* **152** A439–44
[6] Fukui T, Ohara S, Naito M and Nogi K 2001 *J. Chem. Eng. Japan* **34–37** 964–6
[7] Zhu W Z and Deevi S C 2003 *Mater. Sci. Eng.* A **362** 228–39
[8] Primdahl S and Mogensen M 2002 *Solid State Ion.* **152/153** 597–608
[9] Jiang S P, Zhang S, Zhen Y D and Wang W 2005 *J. Am. Ceram. Soc.* **88** 1779–85
[10] Oishi N, Atkinson A, Brandon N P, Kilner J A and Steele B C H 2005 *J. Am. Ceram. Soc.* **88** 1394–6
[11] Dongare M K, Dongare A M, Tare V B and Kemnitz E 2002 *Solid State Ion.* **152/153** 455–62
[12] Lu Z, Pei L, He T-M, Huang X-Q, Liu Z-G, Ji Y, Zhao X-H and Su W-H 2002 *J. Alloys Compounds* **334** 299–303
[13] Mocala K and Navrotsky A 1989 *J. Am. Ceram. Soc.* **72** 826–32
[14] Akande A J, Idem R O and Dalai A K 2005 *Appl. Catal.* A **287** 159–75
[15] Augusto Costa Dias J and Assaf J M 2005 *J. Power Sources* **139** 176–81
[16] Li B, Watanabe R, Maruyama K, Nurunnabi M, Kunimori K and Tomishige K 2005 *Appl. Catal.* A **290** 36–45
[17] Ferdous D, Dala A K and Adjaye J 2005 *J. Mol. Catal.* A **234** 169–79
[18] Andreozzi G B and Princivalle F 2002 *Am. Mineral.* **87** 838–44
[19] Yu Lavrentiev M, Purton J A and Allan N L 2003 *Am. Mineral.* **88** 1522–31
[20] Roelofsen J N and Peterson R C 1992 *Am. Mineral.* **77** 522–8
[21] Halevy I, Dragoi D, Üstündag E, Yue1 A F, Arredondo E H, Hu J and Somayazulu M S 2002 *J. Phys.: Condens. Matter* **14** 10511–6
[22] Rodriguez-Carvajal J 1998 *Program Fullprof98, version 0.2* Laboratorie Leon Brillouin (CEA-CNRS)
[23] *Standard Reference Material 674a, January 15, 1989* Department of Commerce United States of America, National Institute of Standards and Technology
[24] JCPDS-International Centre for Diffraction Data, Copyright (C) JCPDS-ICDD 2000, card 04-0835
[25] JCPDS-International Centre for Diffraction Data, Copyright (C) JCPDS-ICDD 2000, card 30-1468
[26] JCPDS-International Centre for Diffraction Data, Copyright (C) JCPDS-ICDD 2000, card 10-0339
[27] Porta P, Stone F S and Turner R G 1974 *J. Solid State Chem.* **11** 135–47
[28] International Tables for Crystallography, 1996
[29] Jette E R and Foote F 1935 *J. Chem. Phys.* **3** 605–16
[30] Yousuf M, Sahu P C, Jajoo H K, Rajagopalan S and Govinda Rajan K 1986 *J. Phys. F: Met. Phys.* **16** 373–80
[31] Lamas D G and Walsoe de Reca N E 2000 *J. Mater. Sci.* **35** 5563–7
[32] O'Neill H St C and Navrotsky A 1983 *Am. Mineral.* **68** 181–94
[33] Kim J-H, Song R H, Song K-S, Hyun S-H, Shin D-R and Yokokawa H 2003 *Solid State Ion.* **122** 138–43
[34] Kima S D, Hyuna S H, Moona J, Kima J-H and Song R H 2005 *J. Power Sources* **139** 67–72

[35] Swartz S L 2001 Low cost manufacturing of multi-layer ceramic fuels *Solid State Energy Conversion Alliance 2nd Annual Workshop Proc. (March 2001)*
[36] *Fuel Cell Handbook* 2002 6th edn US Department of Energy, Office of Fossil Energy, National Energy Technology Laboratory
[37] Lee J-H, Moon H, Lee H-W, Kim J, Kim D-D and Yoon K-H 2002 *Solid Sate Ion.* **148** 15–26
[38] He T, Lu Z, Pei L, Huang X, Liu Z and Su W 2002 *J. Alloys Compounds* **333** 231–6
[39] Hong H S, Chae U-S, Choo S-T and Lee K S 2005 *J. Power Sources* **149** 84–9
[40] Pratihar S K, Das Sharma A and Maiti H S 2006 *Mater. Chem. Phys.* **96** 388–95